

The Mass Dependence of H α Emission and Stellar Spindown for Fully Convective M Dwarfs

EMILY K. PASS ¹, DAVID CHARBONNEAU ¹, DAVID W. LATHAM ¹, PERRY BERLIND¹, MICHAEL L. CALKINS ¹,
GILBERT A. ESQUERDO ¹ AND JESSICA MINK ¹

¹*Center for Astrophysics | Harvard & Smithsonian, 60 Garden Street, Cambridge, MA 02138, USA*

(Received January 17, 2024)

Submitted to ApJ

ABSTRACT

Fully convective M dwarfs typically remain rapidly rotating and magnetically active for billions of years, followed by an abrupt and mass-dependent transition to slow rotation and quiescence. A robust understanding of this process is complicated by difficulties in estimating M-dwarf ages and potential dependencies on other variables such as birth environment or metallicity. To isolate the effect of mass, we consider M dwarfs in wide binaries. We identify 67 widely separated, fully convective (0.08–0.35M_⊙) M-dwarf binary systems using Gaia and measure the H α feature for each component. We classify the pairs into three categories: systems where both components are active, systems where both are inactive, and candidate transition systems, where one component is active and the other inactive. We gather higher-resolution spectra of the candidate transition systems to verify that their behavior does not result from an unresolved third component, yielding one new triple with surprising activity levels. Neglecting this triple, we find 22 active, 36 inactive, and 8 transition pairs. Our results are consistent with the epoch of spindown for these binaries being primarily determined by mass, with mild second-order effects; we place a 1 σ upper limit of 0.5Gyr or 25% on the dispersion in the mass-dependent spindown relation. Our findings suggest that the large dispersion in spindown epoch previously observed for field stars of a given mass may stem from differences in birth environment, in addition to modest intrinsic stochasticity. We also see evidence that the wide binary population is dispersed over time due to dynamical processing.

1. INTRODUCTION

Sun-like stars begin their lives rotating rapidly and gradually spin down over time as they shed angular momentum. The field of gyrochronology – estimating the ages of stars from their rotation period – is built upon this principle (Skumanich 1972). However, fully convective M dwarfs do not behave like Sun-like stars. Rather, field M dwarfs display bimodal rotation periods, with few interlopers located between the modes. This result implies that there is an abrupt transition between short (< 10 day) and long (> 70 day) rotation periods; from galactic kinematics, the transition is inferred to occur at ages of a few billion years on average, although it is mass dependent (Newton et al. 2016, 2018).

Even within a mode, gyrochronological principles may not apply; that is, a more slowly rotating M dwarf may be younger than a more rapidly rotating one. In Pass et al. (2022), we studied M dwarfs in wide binaries with stars of known age in an attempt to probe the time dependence of spindown. We found that while there

is gradual spindown within the rapidly rotating mode over a few billion years – which would be promising for gyrochronology – the dispersion in initial rotation rates is similarly large, likely stemming from differences in the disk lifetime and subsequent disk-locking early in the star’s life (e.g., Rebull et al. 2018). A fully convective M dwarf with a 5-day rotation period could therefore be very young with slow initial rotation, or it could be a few gigayears old and gradually spinning down from a faster initial rate. In that work, we also found that the time of transition between modes can vary greatly from star to star, with some 0.2–0.3M_⊙ M dwarfs making the jump by 600Myr and others remaining rapidly rotating for gigayears. There is therefore no guarantee that a specific star in the slowly rotating mode is older than a specific star in the rapidly rotating one, although the slowly rotating population is older on average.

While the spindown of fully convective M dwarfs is complicated, understanding this process is a worthwhile pursuit, particularly in the context of exoplanets: fully

arXiv:2401.10167v1 [astro-ph.SR] 18 Jan 2024

convective M dwarfs host the only terrestrial exoplanets whose atmospheres are amenable to characterization with current and near-future instrumentation, such as JWST and the ELTs (e.g., Snellen et al. 2013; Lovis et al. 2017; Morley et al. 2017). Stellar rotation and activity are closely correlated (Kiraga & Stepien 2007), including X-ray emission (Wright et al. 2011, 2018), H α emission (Newton et al. 2017), UV emission (France et al. 2018), and flare rate (Medina et al. 2020, 2022b). An M dwarf that remains in the rapidly rotating mode for gigayears therefore subjects its attendant planets to a violent environment of high-energy photons and, likely, a corresponding high flux of charged particles for gigayears, decreasing the feasibility of atmosphere retention (e.g., Lammer et al. 2007; Tilley et al. 2019). A robust understanding of the spin and activity evolution of fully convective M dwarfs is therefore necessary to accurately model the evolution of planetary atmospheres.

Stellar mass is known to have a significant impact on the age at which a fully convective M dwarf transitions between rotation/activity modes (Newton et al. 2016, 2017, 2018; Medina et al. 2022b); to what extent do other variables play a role? While we attempted to investigate this question in Pass et al. (2022) by studying the rotation of M dwarfs in wide binary pairs with other M dwarfs, our conclusions were limited by selection biases, as it is much easier to measure short rotation periods than long ones.

In this work, we take a different approach to avoid incompleteness. As mentioned above, activity is an excellent proxy for rotation: using a volume-complete survey of single, low-mass M dwarfs, we found that $92\pm 3\%$ of $0.1\text{--}0.3M_{\odot}$ M dwarfs that are active in H α have rotation periods shorter than 20 days (Pass et al. 2023b), with the remaining $8\pm 3\%$ also having shorter rotation periods than the typical >100 -day periods of slow rotators (see Figure 5 of Pass et al. 2023b). By measuring H α emission for each component in wide M-M binary pairs, we can therefore probe the mass dependence of stellar spin-down: does the more massive component always spin down first, or are there other factors at play? This observing strategy also controls for some variables, as binary stars likely formed together and therefore share their metallicity (Desidera et al. 2004, 2006) and birth environment.

In Section 2, we discuss our observing strategy: Section 2.1 presents our target selection with Gaia, Section 2.2 our initial observing campaign with the mid-resolution FAST spectrograph, Section 2.3 our follow-up campaign with the higher-resolution TRES spectrograph, and Section 2.4 the characterization of an intriguing new triple system. We discuss our results in

Section 3 and conclude in Section 4.

2. OBSERVATIONS

2.1. Target selection

To select our targets, we conduct a search for common proper motion (cpm) pairs within 50pc from Gaia EDR3 (Gaia Collaboration et al. 2016, 2021; Lindegren et al. 2021), following a similar procedure to that outlined in Pass et al. (2022). That is, we cross-match with the 2MASS catalog (Cutri et al. 2003), discard sources with absolute K -band magnitudes outside the range appropriate for M dwarfs ($5 < M_K < 10$ mag), and estimate masses for each remaining source using the Benedict et al. (2016) K -band mass-luminosity relation. This relation has an rms scatter of $\pm 0.014M_{\odot}$. We identify cpm pairs using the proper motion ratio and proper motion position angle difference cuts of Montes et al. (2018, i.e., a threshold of 0.15^2 in their Equation 1 and 15° in their Equation 2). We also require parallax agreement within 0.4mas; this is a slightly tighter constraint than the 2mas threshold used in Pass et al. (2022), as we found in that work that such a lenient cut results in false positives in the form of single Hyads.

We further limit our list of cpm pairs given the science goals of this investigation. As we are interested specifically in fully convective M dwarfs, we remove sources with estimated masses outside the range $0.08\text{--}0.35M_{\odot}$. We also remove one target that we identify as a white dwarf based on its $G_{BP} - G_{RP}$ color. From inspection of previous measurements from Newton et al. (2017), we assume sources fainter than $m_R = 15.5$ mag will be unsuitable for H α analysis with FAST; we therefore also limit our search to sources brighter than this threshold, with R -band magnitudes estimated using the empirical $G - K$ color relation from Winters et al. (2021). We require that the components have separations between 4 and 2000", with the lower threshold representing our ability to resolve the targets with FAST under typical seeing and the upper boundary intended to mitigate false positives at extremely wide separations. Note that our results are insensitive to the exact choice of upper boundary, as we do not identify any pairs with separations between 1000–2000". We cut stars with Gaia EDR3 renormalised unit weight error (RUWE) values greater than 2; this quantity represents the excess noise in the Gaia astrometric solution, with values substantially larger than 1 suggesting that the star is likely an unresolved binary. We also only consider targets above declination -15° to ensure all sources are easily accessible from our telescope.

This search yields 66 pairs. We also manually add LHS 3808 / LHS 3809 to our target list, for a to-

tal of 67 pairs. These stars are missing from the `gaiadr2.tmass.best_neighbour` crossmatch table (Marrese et al. 2019) that we use to obtain K -band magnitudes and therefore were not found by the above algorithm, but they nonetheless meet the criteria outlined above.

2.2. FAST observations

Our goal is to measure the H α feature for each component in our 67 wide-binary, mid-to-late M dwarfs pairs, and thus identify informative “transition” systems in which one star is active and the other inactive. To this end, we observed each star with the FAST spectrograph (Fabricant et al. 1998) at the 1.5m Tillinghast Reflector at the Fred Lawrence Whipple Observatory, with our observing campaign beginning in 2022 May and concluding in 2023 November. We reduced the spectra using the instrument’s standard pipeline (Tokarz & Roll 1997). Our campaign used the same settings as a previous search for H α emission in a different sample of M dwarfs, described in Newton et al. (2017). Specifically, we attained roughly $R = 3000$ resolving power over a wavelength range of 5550–7550Å. We selected exposure times with the goal of attaining a per-pixel SNR of 40 in the continuum near the 6563Å H α feature to ensure a clear detection of emission, if present.

We measure the equivalent width of the H α feature using the method described in Newton et al. (2017), defining the feature as the wavelength range 6558.8–6566.8Å and the continuum regions as 6500–6550Å and 6575–6625Å. We adopt the convention that a negative equivalent width indicates emission.

Newton et al. (2017) used -1Å as their threshold to distinguish between active and inactive M dwarfs from FAST spectra, although a related study with the same instrument placed the boundary at -0.75Å (West et al. 2015). Newton et al. (2017) noted that there were few stars in their sample with equivalent widths between -0.5Å and -1.5Å and so the exact value selected for this threshold is not strongly motivated. We therefore classify our stars as follows:

- **Inactive:** If both stars in a pair have H α in absorption or negligible H α emission ($H\alpha > -0.5\text{Å}$), the pair is considered inactive. That is, these are likely older stars that have already spun down to slow rotation and magnetic quiescence.
- **Active:** If both stars have obvious H α emission ($H\alpha < -1\text{Å}$), the pair is considered active. That is, these are likely young, rapidly rotating stars with substantial magnetic activity.
- **Candidate Transition:** Pairs that do not fall into either of the above categories are candidate

transition systems. In some cases, one star is clearly active and the other inactive; in others, the equivalent widths are near the activity threshold and higher-resolution follow up would be beneficial to confirm whether an emission feature is present in one or both stars.

2.3. TRES observations

As we showed in Pass et al. (2022), hierarchical triples like GJ 1006 and GJ 1230 can masquerade as transition systems, where one component remains active at an advanced age because activity and rotation are maintained by tidal interactions with a close binary companion; G 68-34 (Pass & Charbonneau 2023) is another example of such a system, where a spin-orbit synchronized pair of fully convective M dwarfs have maintained rapid rotation and H α activity for over 5Gyr due to binary interactions. Our target selection uses a cut on Gaia RUWE to avoid many unresolved binaries, but there are some binary configurations for which we would not expect an astrometric perturbation (e.g., equal-mass binaries or very short-period binaries).

We therefore follow up the eleven candidate transition systems using the higher-resolution ($R = 44000$) TRES spectrograph at the same 1.5m telescope to confirm the H α emission levels observed by FAST and vet the stars for unresolved binarity. We search for double lines in both stars, and obtain a second TRES observation for the active star in each pair after a few days to check for radial-velocity variability. To reduce the TRES observations and extract these radial velocities, we use our mid-to-late M-dwarf pipeline described in Pass et al. (2023a).

Our TRES follow up yields one intriguing new triple system, which we discuss in Section 2.4. We reclassify one system as active, one as inactive, and confirm that the remaining eight are transition systems with no evidence for unresolved binary companions. The final classification criteria are therefore:

- **Inactive:** Both stars have $H\alpha > -0.5\text{Å}$.
- **Active:** Both stars have $H\alpha < -1\text{Å}$.
- **Transition:** One star has $H\alpha > -0.5\text{Å}$ and the other has $H\alpha < -1\text{Å}$.

We tabulate the 8 transition systems in Table A1, the 22 active systems in Table A2, and the 36 inactive systems in Table A3, for a total of 66 pairs. The 67th system is the newly discovered triple and is discussed separately, below. The tables include the 2MASS IDs of the components, the distance from Earth, the angular separation between components, the masses and

mass difference between components, the H α equivalent widths measured by FAST, and (where applicable) the H α equivalent widths measured by TRES. While we include our nominal measurement uncertainty for the FAST equivalent widths, note that astrophysical variation in this feature over time is likely to introduce substantially larger uncertainties (e.g., Medina et al. 2022a).

2.4. LDS 942: an intriguing new triple

The cpm pair 2MASS J12565215+2329501 and 2MASS J12565272+2329506 was known to be a binary long before Gaia, appearing in the Luyten Double Star catalog as LDS 942A and B (Luyten 1969). Following our target selection described in Section 2.1, we identify this pair as comprising a roughly equal-mass binary ($0.334M_{\odot}$ and $0.324M_{\odot}$), located at a distance of 27pc from Earth and with the components separated by $8''$, implying a projected physical separation of 220au. With FAST, we measure H α equivalent widths of $-0.731\pm 0.016\text{\AA}$ for A and $-4.516\pm 0.028\text{\AA}$ for B. We therefore flag the pair as a candidate transition system, causing us to pursue follow up observations with TRES.

Given our motivation set forth in Section 2.3, we thought it possible that LDS 942B might be an unresolved binary, with its H α activity explained by binary interactions between two close components. However, we did not observe double lines in the TRES spectra of this star, nor statistically significant RV variation in five epochs of observations taken over a span of two months. The five observations have a sample standard deviation of 75ms^{-1} , providing a tight constraint on the possible existence of close companions. The star is thus presumably single (exempting its wide companion, LDS 942A).

We also collected an observation of LDS 942A to verify the H α equivalent width we observed in the FAST spectrum and were surprised to find that the A component was a double-lined spectroscopic binary. We continued to collect a total of ten TRES spectra of A in 2023 March/April in order to determine the orbit of the newly discovered LDS 942AC.

We follow the method of Winters et al. (2020) to extract radial velocities of double-lined spectroscopic binaries from TRES spectra, which is based on the TODCOR technique (Zucker & Mazeh 1994). This analysis uses TRES order 41, corresponding to wavelengths of 7065–7165 \AA . As in Winters et al. (2020), we use a spectrum of Barnard’s Star as the template for our cross correlation. We tabulate our extracted radial velocities in Table 1. This analysis yields a C/A light ratio of 0.73 and no discernible rotational broadening for either star at the resolution of the spectrograph (i.e., $v\sin i < 3.4\text{kms}^{-1}$).

Table 1. TODCOR results for LDS 942A and C

BJD [d]	RV _A [kms ⁻¹]	RV _C [kms ⁻¹]	<i>h</i>	<i>t</i> _{exp} [s]
2460007.8388	-4.254	-15.311	0.833	3600
2460016.8462	-46.525	33.585	0.889	3600
2460030.8208	0.623	-20.402	0.857	3600
2460036.7726	-16.468	-0.885	0.939	3600
2460042.7963	-35.849	21.387	0.911	1800
2460045.8009	1.725	-21.731	0.891	1800
2460053.7711	4.129	-24.326	0.866	1800
2460057.8406	-3.051	-16.583	0.845	1800
2460062.8897	-20.496	4.121	0.896	1950
2460064.7879	-34.034	19.180	0.918	1950

NOTE—*h* is the cross-correlation coefficient

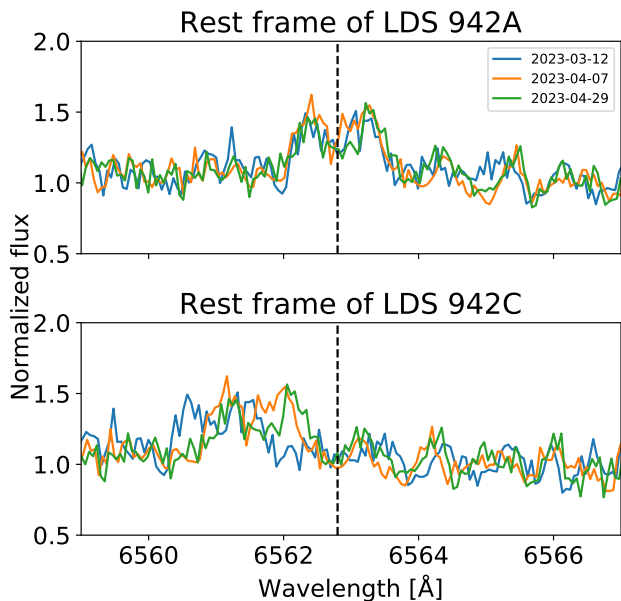


Figure 1. The 6563 \AA H α feature (dashed line) in the blended spectrum of LDS 942AC, as observed by TRES. For clarity, we show only the epochs in which the lines of the two components are separated by at least 50kms^{-1} . In the upper panel, we have shifted the spectra to the rest frame of LDS 942A, and in the lower panel, to the rest frame of C. An H α emission feature is present in the spectrum of LDS 942A. The C component does not show any obvious emission.

On the other hand, the spectra of LDS 942B are rotationally broadened, with $v\sin i = 5.8\text{kms}^{-1}$. LDS 942ABC was observed by the Transiting Exoplanet Survey Satellite (TESS; Ricker et al. 2015) in two sectors, with all three stars falling into the same TESS pixel; we observe a clear rotation period of 2.55 days in this blend and no other significant periodogram signals aside from harmonics of this period. Given our $v\sin i$ measurements, LDS 942B is likely the source of this modulation: a mass

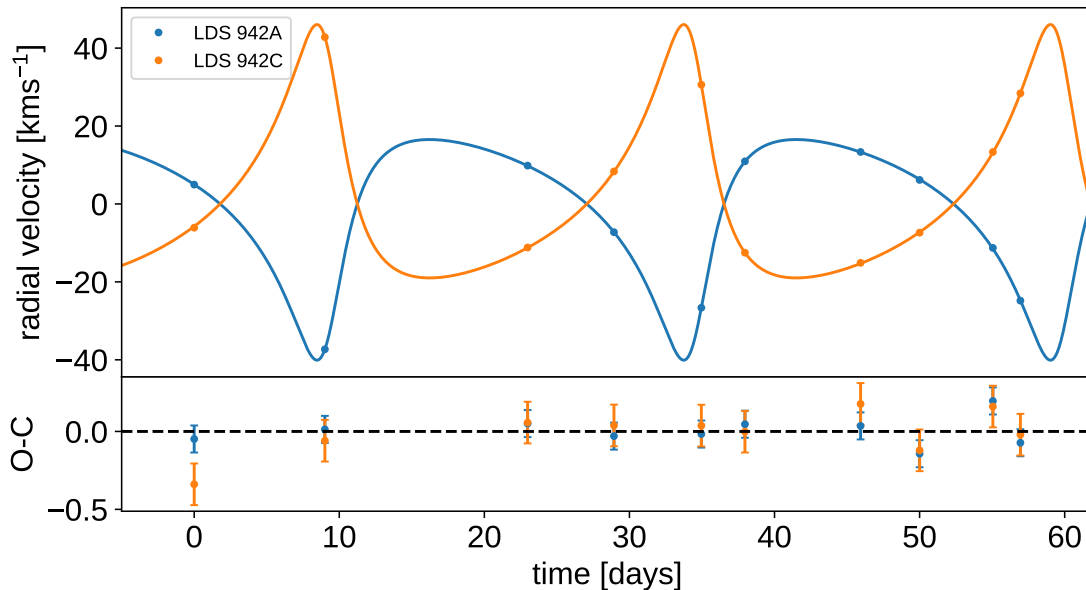


Figure 2. Our maximum *a posteriori* orbital solution for the newly discovered close binary, LDS 942AC. The fit has a period of 25.27 ± 0.02 days and a substantial eccentricity of 0.501 ± 0.002 .

of $0.324 M_{\odot}$ would imply a radius of $0.321 R_{\odot}$ using the mass–radius relation of Boyajian et al. (2012), yielding an equatorial velocity 6.4 km s^{-1} for a rotation period of 2.55 days. Considering an isotropic distribution of spin axes, the median value for $\sin i$ is $\sin(60^{\circ}) = 0.87$; this value would yield an observed rotational broadening of roughly 5.5 km s^{-1} , close to the $v \sin i$ we measure for LDS 942B. The rotation periods of the other two stars remain unknown.

Our TRES observations of LDS 942B yield a median H α equivalent width of -4.15 \AA , measured following the method of Medina et al. (2020). This value is comparable to the -4.52 \AA equivalent width measured for this star from the FAST spectrum. For the blended LDS 942AC spectrum, the high resolving power of TRES allows us to measure the H α features individually for the two blended components. In Figure 1, we show the three of our LDS 942AC spectra in which the two sets of lines are most separated. Inspection of these spectra reveals obvious H α emission in LDS 942A and no such signature in LDS 942C. Using these three spectra, we measure a median equivalent width of -0.83 \AA for A in the blended spectrum; considering our TODCOR light ratio of 0.73, this measurement implies that the equivalent width would be -1.44 \AA in a deblended spectrum of A. We note that if we take the median of our measurement for A in all ten spectra, we obtain a similar value of -0.78 \AA in the blended spectrum; there therefore does not appear to be any additional H α emission introduced by component

Table 2. Orbital fit for LDS 942AC

Parameter	Value	Error	Unit
P	25.274	0.016	days
T_{peri}	2460017.016	0.019	BJD
e	0.5013	0.0020	—
ω	214.01	0.27	$^{\circ}$
γ	-9.22	0.50*	km s^{-1}
$K_A + K_C$	60.77	0.31	km s^{-1}
$M_A \sin^3 i$	0.2035	0.0028	M_{\odot}
$M_C \sin^3 i$	0.1772	0.0024	M_{\odot}
q	0.8707	0.0031	—
σ_A	0.129	0.031	km s^{-1}
σ_C	0.160	0.025	km s^{-1}

NOTE—*This error is dominated by the uncertainty in our determination of the absolute zero point of the TRES RV scale, resulting from the absolute RV error in a comparison spectrum of Barnard’s Star (Winters et al. 2020). Relative RVs are known to much greater precision.

C, suggesting that C is H α inactive. We do not make a quantitative measurement of its H α equivalent width given the uncertainties introduced by the blend.

We use `exoplanet` (Foreman-Mackey et al. 2021) to fit an orbital solution to our TODCOR radial velocities (Figure 2). We allow the RV uncertainties to be free parameters of the fit, with each of the ten observations having the same error but with a different value for the two stellar components. We identify the maximum *a posteriori* (MAP) solution with `exoplanet`, then use `PyMC3`

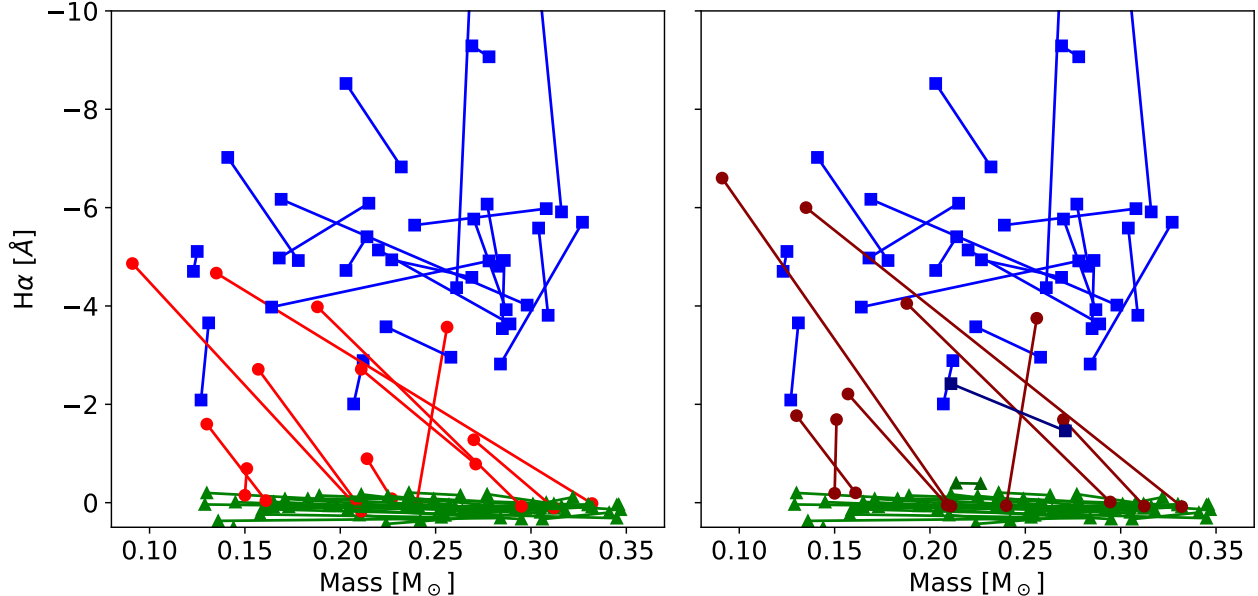


Figure 3. The $H\alpha$ equivalent widths for our 66 pairs, excluding the newly discovered triple. The two components are joined by a line. The left panel shows our original FAST observations. Active pairs are noted with blue squares, inactive pairs with green triangles, and candidate transition systems with red circles. In the right panel, we replace the measurements for the candidate transition systems with our follow-up observations from TRES, with red now denoting confirmed transition systems. We use a darker shade of each color in this plot to indicate the pairs with refined equivalent widths from TRES follow up.

(Salvatier et al. 2016) to sample the posterior, starting from the MAP solution and using two chains each with a 1500 draw burn-in and 2000 draws. The orbital parameters inferred from this analysis are given in Table 2.

Our spectroscopic fit yields a mass ratio of $q = 0.87$. To estimate the masses of the individual components, we assume the TRES light ratio approximates the light ratio in R band. We use the deblending ratio from Riedel et al. (2014) to convert to a K -band light ratio, deblend the observed K -band magnitude into its two components, and apply the Benedict et al. (2016) relation to obtain component masses, yielding $0.23M_{\odot}$ and $0.20M_{\odot}$. These component masses are fully consistent with the spectroscopically determined mass ratio, implying an inclination of roughly 70° .

LDS 942B is therefore the brightest and most massive star in the system, with a mass of $0.32M_{\odot}$. It is in the active phase of its life, with a short rotation period of 2.55 days and substantial $H\alpha$ emission (-4.15\AA). Its widely separated companion LDS 942A is fainter and less massive, with a mass of $0.23M_{\odot}$, no observed rotational broadening, and modest $H\alpha$ emission (-1.44\AA). LDS 942C is a close companion to A and the faintest and least massive star in the system, with a mass of $0.20M_{\odot}$. It does not show any rotational broadening and appears to be inactive in $H\alpha$. The AC pair has a short and eccentric 25-day orbit.

Given our expectation that more massive M dwarfs spin down at younger ages, this system is unusual: the most massive component remains active and rapidly rotating, while the least massive component appears to have spun down (or at least, is magnetically quiescent). It is known that spin-orbit synchronization can lead to M dwarfs with anomalously long-lived rapid rotation and activity (e.g., Pass & Charbonneau 2023); the LDS 942 system may hint that multiplicity can have even more insidious influences on the population of M dwarfs. That is, there may also be types of binary interactions that drive systems to longer rotation rates and magnetic inactivity. For example, Felce & Fuller (2023) discuss another spin-orbit equilibrium in which interactions from an outer companion drive an inner close binary into Cassini state 2, leading to very slow rotation. Future photometric monitoring of the LDS 942AC pair to determine the rotation periods of these components may therefore lead to new insights into the influence of stellar interactions on spindown and activity.

3. DISCUSSION

3.1. Transition systems are less active

Our $H\alpha$ equivalent widths for our 66 pairs (exempting the LDS 942 system) are shown in Figure 3. Inspecting the FAST observations in the left panel, we see that the active stars in the transition systems tend to have

weaker H α emission than stars in active pairs: nearly half of the stars in active pairs have H α emission stronger than -5\AA as measured by FAST, while none of the stars in transition pairs do. This effect is less pronounced in the right panel, but that figure includes data from two different instruments; the larger H α features for the transition systems observed from TRES suggest that there may be some differences between the data sets, as different continuum regions are used to measure the feature given the dramatically different resolving powers of the two spectrographs.

In our investigation of a volume-complete sample of single, H α -active mid-to-late M dwarfs in Pass et al. (2023b), we observed a likely related phenomenon (Figure 6 of that work): stars with longer rotation periods within the rapidly rotating mode (periods of 2–10 days) tended to have lesser levels of H α emission than stars with the shortest rotation periods (periods less than 0.5 days), suggesting that H α emission tempers over time as M dwarfs spin down gradually within the rapidly rotating mode. This explanation suits our findings in this M–M binary sample: pairs in which one component has already spun down are likely to be older, and hence the remaining active component has had time to undergo substantial spindown, even though it has not made the jump to the slowly rotating sequence yet.

3.2. A simple model of fully convective M-dwarf spindown

While Figure 3 is qualitatively interesting, we wish to make a more quantitative statement: is this distribution of pairs consistent with the epoch of spindown being determined solely by stellar mass? To answer this question, we can use the volume-complete sample of single, 0.1–0.3 M_{\odot} M dwarfs within 15pc (Winters et al. 2021; Pass et al. 2023a,b) to construct a simple model of the mass dependence of spindown (Figure 4). As this sample is volume complete, the active fraction as a function of mass is proportional to the average age of transition between modes, with the conversion requiring an assumption on star formation history. We follow Medina et al. (2022b) and assume that star formation has been constant over the last 8Gyr, which is motivated by the results of Fantin et al. (2019) for the galactic thin disk (note that our solar neighborhood overwhelmingly comprises thin disk stars; using Gaia kinematics and the method described in Medina et al. 2022b, we find that only five pairs in our sample are more likely to be members of the thick disk than the thin disk).

Figure 4 shows that the M-dwarf active fraction – and hence, the average age of transition – scales roughly lin-

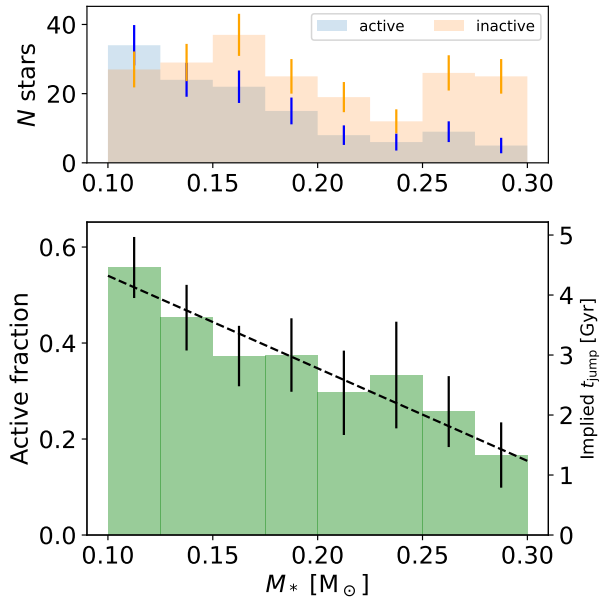


Figure 4. The upper panel shows a histogram of the single stars in the volume-complete sample of mid-to-late M dwarfs (Winters et al. 2021), with the inactive sample taken from Pass et al. (2023a) and the active sample from Pass et al. (2023b). The lower panel shows the fraction of stars that are active. We find that this fraction is roughly linear with mass, following the trend $f = 0.73 - 1.93M_*/M_{\odot}$.

early with mass. For the active fraction, this is:

$$f(M_*) = 0.73 - 1.93M_*/M_{\odot}, \quad (1)$$

or for the time of transition:

$$t_{\text{jump}}(M_*) = 5.9 - 15.4M_*/M_{\odot}. \quad (2)$$

A linear relationship implies that the probability of observing a pair in transition between the modes is proportional to the difference in mass between the components. By taking the derivative of Equation 1, we find that the probability of observing a system in transition is:

$$P(\Delta M_*) = 0.193 \frac{\Delta M_*}{0.1M_{\odot}}; \quad (3)$$

i.e., there is a 19% chance that a pair would be observed in transition if the component masses differ by $0.1M_{\odot}$.

3.2.1. Evaluating the model at the population level

Is our M-M binary sample consistent with this simple model? For each pair, we assign an age from a random uniform distribution spanning 0–8Gyr. For each component, we calculate t_{jump} given its mass; if the star is older than this value, we consider it inactive, and if it

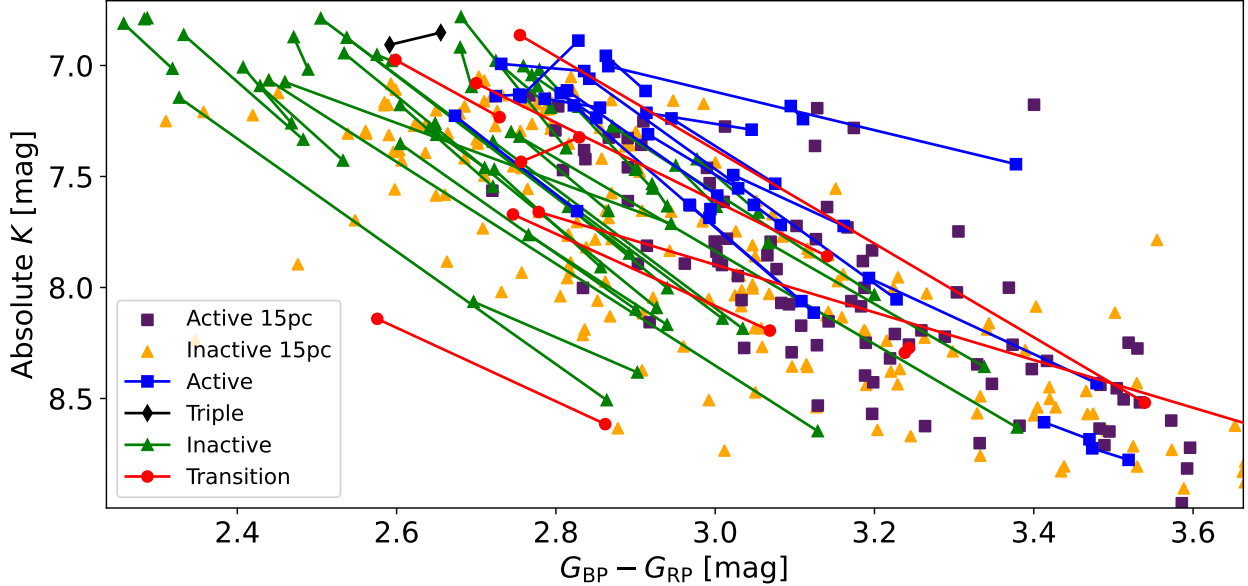


Figure 5. A color-magnitude diagram of our M-M binary pairs, overplotted on the volume-complete sample of single $0.1\text{--}0.3M_{\odot}$ M dwarfs within 15pc (from Figure 10 of [Pass et al. 2023b](#)). The eight transition systems are shown in red. The axes provide the Gaia $G_{BP} - G_{RP}$ color and absolute K -band magnitude, which combines 2MASS apparent magnitude and Gaia parallax.

is younger, we consider it active. We repeat this simulation 1000 times, recording the number of active, inactive, and transition pairs that we obtain. This exercise yields 14.3 ± 3.3 active pairs, 45.0 ± 3.8 inactive pairs, and 6.7 ± 2.3 transition pairs. While the number of transition pairs is in agreement, the simple model predicts significantly fewer active pairs and more inactive pairs than we observed (which were 22 and 36, respectively).

Note that while we performed these calculations in terms of age for ease of explanation, we could alternatively have done so entirely in terms of active fraction; the assumption we make about the star formation rate cancels out, as it is applied to both our equation for t_{jump} and our assigned ages. The discrepancy therefore cannot be explained by an inaccurate assumption of that history (although we are assuming that the star formation history for single stars within 15pc is the same as for binaries within 50pc).

A possible explanation for our overabundance of active systems is selection bias: our target selection is magnitude limited (unlike the volume-complete sample), and young stars are overluminous. To investigate this possibility, we rerun our Gaia target selection algorithm but remove the requirement that stars must be brighter than $m_R = 15.5$ mag. This change would nearly double our sample size, meaning that a preferential selection of young, overluminous stars could have an impact on our sample. However, we would not expect the difference to be dramatic: if one assumes that these M dwarfs would

be overluminous for 300Myr (see discussion in [Pass et al. 2022](#)) and star formation has been uniform for 8Gyr, 4% would be overluminous; even if their overluminosity caused all of them to enter our sample, this bias would only result in three additional active systems. We also vet our sample for members of young moving groups using the BANYAN Σ tool ([Gagné et al. 2018](#)) and radial velocities, proper motions, and parallaxes from Gaia. All but two of the pairs are most likely field stars and therefore unlikely to be overluminous. One pair, 2MASS J03513447+07222250 and 2MASS J03513420+0722229, is likely a member of the Hyades with age 600–800Myr ([Brandt & Huang 2015](#)); we also do not expect overluminosity at this age. The other pair has a high membership probability for the Carina-Near Moving Group, for which overluminosity would be expected, but as we discuss in Section 3.3.2, past work has argued that the Carina-Near classification is incorrect for this system and the pair actually belongs to the field.

Figure 5 shows a color-magnitude diagram of our sample, overplotted on the volume-complete 15pc sample of single, $0.1\text{--}0.3M_{\odot}$ M dwarfs from [Pass et al. \(2023a,b\)](#). This figure is consistent with our discussion thus far: there is a handful of active systems whose positions could be consistent with overluminosity (located in the upper right of the figure), but most do not appear to be overluminous. The active pairs do tend to be redder than the inactive pairs at constant luminosity, but this is also observed in the volume-complete sample and

may be the result of starspot coverage (e.g., Covey et al. 2016). To confirm that differences in starspot coverage could feasibly generate the offsets we observe, we examine the stellar evolutionary models of Somers et al. (2020), which include the structural effects of starspots. We use $V - I_c$ as a proxy for $G_{BP} - G_{RP}$, as Gaia colors have not been calculated for low-mass M dwarfs in the Somers et al. (2020) grid for $f_{\text{spot}} \neq 0$. For a $0.3M_{\odot}$ M dwarf, these models predict a 0.54 mag difference between stars with $f_{\text{spot}} = 0$ and $f_{\text{spot}} = 0.85$, the minimum and maximum values modelled. A more modest difference in starspot filling fraction could therefore explain the observed data; for example, the $f_{\text{spot}} = 0.34$ and $f_{\text{spot}} = 0.68$ models are separated by an offset of roughly 0.2 mag.

Another possible explanation for our overabundance of active stars is unresolved binarity. While we have carefully vetted our transition systems for unresolved companions, the active pairs have not been followed up with a higher resolution spectrograph. Winters et al. (2019) showed that roughly 20% of M-dwarf systems consist of a close binary with separations less than 50au, although this fraction does decrease for low-mass M dwarfs. Some of these close binaries would also produce astrometric perturbations and hence be rejected by our cut on Gaia RUWE; nonetheless, some would be missed, as with LDS 942AC. However, this effect could not turn an inactive system into an active system unless both components were unresolved binaries, which would be unlikely; the fact that we did not identify an abundance of unresolved binaries in our TRES follow-up of transition pairs therefore disfavors this hypothesis. On the other hand, binarity also acts to change the component masses; unresolved binarity could merely be leading to inflated mass estimates and hence underestimates of the active lifetime. That is, if we were to artificially decrease the masses of some of our active stars, our simulation would predict a greater number of active pairs. However, the color-magnitude diagram in Figure 5 also disfavors an abundance of unrevolved binaries. While there is substantial thickness to the color-magnitude diagram at these low masses, the M-M binary pairs have similar slopes, which is unsurprising if the thickness of the color-magnitude diagram is caused by characteristics shared by both components of the binary, such as age or metallicity. Unresolved triples are likely to have unusual slopes, as potentially both the magnitude and the color of one of the points is incorrect due to the blend. The slopes of the active pairs generally appear similar to those of the inactive pairs (with a handful of exceptions: most notably, LP 196-29 / LP 196-30), again suggesting that an abundance of unresolved binaries is unlikely.

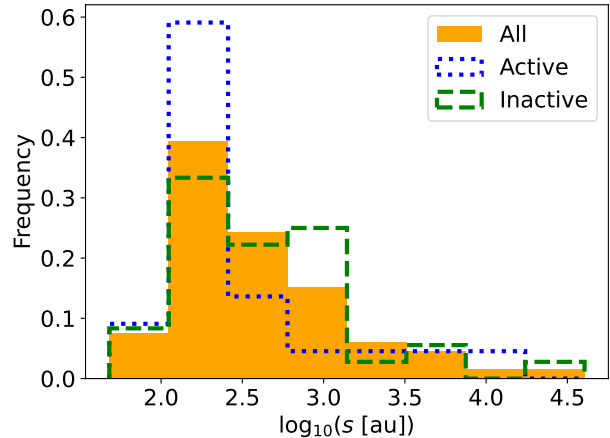


Figure 6. The projected physical separations between binary components. All 66 active, inactive, and transition pairs are included in the orange histogram; the blue dotted line indicates only the active pairs while the green dashed lines shows only the inactive pairs. A KS test yields tentative evidence (77% confidence) that the active and inactive pairs are drawn from different distributions, with the active pairs having preferentially smaller separations.

And of course, unusual slopes do not necessitate binarity; if starspot coverage indeed has a significant impact on the CMD position of a given star, some differences between members of a binary pair might be expected even though metallicity and age are constant.

A remaining possibility is that Equation 1 is different for binaries than it is for single stars. One reason this might occur is if the population of binaries is evolving with time. Such an outcome is expected given Heggie’s Law: interactions with other stars will cause the orbit of a hard (close) binary to harden, and a soft (wide) binary to soften (Heggie 1975). Hardening could cause binaries to evolve to separations smaller than our 4” lower limit, excluding them from our sample selection. Softening orbits could lead to the binary becoming unbound, thereby becoming single stars and also evading our target selection. Considering the density of the field environment, we expect our wide binaries to be soft. In this framework, Equation 1 overpredicts the number of inactive stars we would observe because a subset of the predicted stars are no longer wide binaries in their old age. Alternatively, denser star formation environments in the past could disrupt binaries and cause older stars to have a lower primordial binary fraction (Parker & Meyer 2014; Longmore et al. 2014), although Moeckel & Clarke (2011) argue that the formation of soft binaries in clusters is actually independent of cluster size.

Do we see any indication of dynamical processing? In Figure 6, we show a histogram of the projected separa-

tions for the active and inactive pairs. There is tentative evidence of a statistically significant difference between these populations, with a KS test yielding a 23% chance that the two samples are drawn from the same distribution. The inactive pairs tend towards larger separations than the active pairs. This result could be a signature of dynamical processing: the models of [Jiang & Tremaine \(2010\)](#) that simulate the evolution of wide field binaries due to gravitational perturbations from passing stars find that these interactions shift the separation distribution to wider separations for stars that remain bound, and also result in many pairs becoming unbound. Dynamical processing could therefore explain both the shift in [Figure 6](#) as well as the underabundance of inactive pairs we observe relative to our simple model expectations.

To approximate this effect in our simple model, we make the assumption that the probability of a binary experiencing a disruptive interaction is uniform in time. We therefore modify our age prior: instead of a flat distribution, there is a linear decrease in the likelihood of observing a binary pair at a given age. This treatment requires a normalization that represents the fraction of wide binary pairs that remain undisrupted for 8Gyr. We test a variety of values. We find that if 20% of wide binaries remain in existence for 8Gyr, then we would expect 21.2 ± 3.8 active pairs, 8.8 ± 2.6 transition pairs, and 36.0 ± 4.0 inactive pairs, in agreement with our observations. As a statistical ensemble, our observations are therefore plausibly consistent with a picture in which stellar mass alone determines the age at which a star spins down, at least when metallicity and stellar birth environment are controlled.

To investigate the alternative, we also consider adding a random dispersion to our spindown times. We model this effect by adding an offset drawn from a random normal distribution with $\sigma=1\text{Gyr}$ to [Equation 2](#), with each component receiving a different offset. We still include the dynamical processing described above. This treatment predicts an increase to 14.5 ± 3.4 transition systems, which is disfavored by our observations. A dispersion of 0.5Gyr would yield 10.9 ± 2.9 transition systems, which remains plausible at 1σ . If we instead model the dispersion as a fractional effect, a 25% dispersion in the epoch of spindown also produces agreement within 1σ . In summary, our population-level observations are consistent with either no or modest dispersion.

3.2.2. Evaluating the model for specific systems

The individual transition systems can also grant us additional insights. Two of our observations are nominally impossible given our simple model: 2MASS

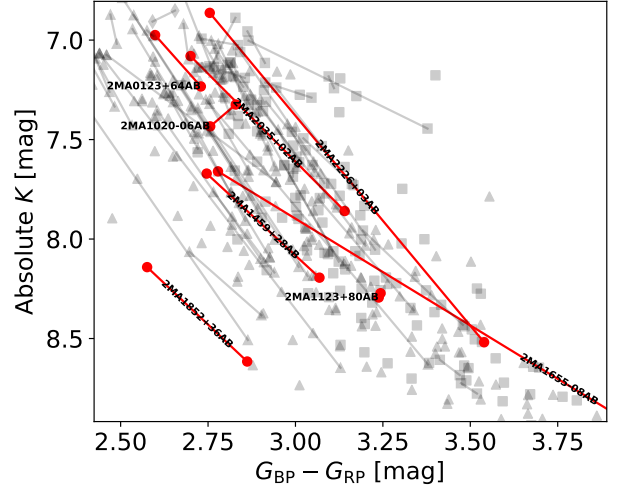


Figure 7. This plot shows the same data as [Figure 5](#), but with the transition systems annotated.

J11231269+8009027 / 2MASS J11231650+8009045 and 2MASS J10204884-0633195 / 2MASS J10205111-0634400, where the less massive component has spun down first. In both cases, the masses of the two components are similar. Considering the $\pm 0.014M_{\odot}$ uncertainty in the [Benedict et al. \(2016\)](#) mass–luminosity relation, it is plausible that we are mistaken in our identification of the more massive component, particularly for 2MA1123+80AB in which the masses are nearly identical. However, the mass difference for 2MA1020-06AB is $0.016M_{\odot}$; while this is only marginally larger than the nominal error in the mass–luminosity relation, [Benedict et al. \(2016\)](#) note that this scatter likely stems from a combination of age, metallicity, and magnetic effects. Our binary pairs presumably share a common age and metallicity, and hence a lesser degree of scatter should be expected than in the relation at large.

Magnetic effects do remain a consideration, although starspot-induced photometric modulation is unlikely to cause the discrepancy: fully convective M dwarfs that are modestly active or inactive have typically photometric peak-to-peak amplitudes of 0.01 mag in the optical ([Pass et al. 2023b](#)), with even smaller amplitudes expected at longer wavelengths (e.g., [Miyakawa et al. 2021](#)). However, differing filling factors of longitudinally homogeneous spots (which do not cause photometric time variation) could play a role (e.g., [Irwin et al. 2011](#); [Jackson & Jeffries 2013](#)). We note that for both of these pairs, the brighter/active component is redder ([Figure 7](#)), a behavior we see generally for both the active stars in this study and for the active single stars in the volume-complete sample from [Pass et al. \(2023b\)](#). On the other hand, work such as [Morrell & Naylor](#)

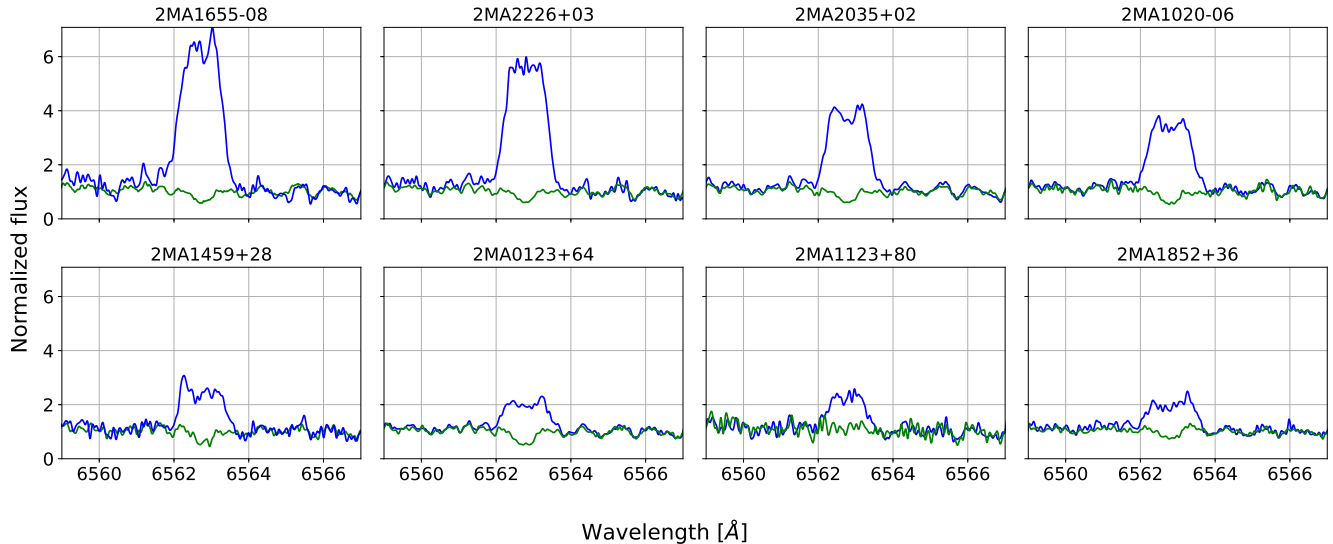


Figure 8. The 6563Å H α feature for our transition pairs, as observed by TRES. The active component is shown in blue and the inactive component in green. Equivalent widths are tabulated in Table A1.

(2019) suggests that there is no statistically significant difference between active and inactive M dwarfs with respect to either starspot coverage or radius inflation, which would disfavor this explanation.

Even if the inactive component in these pairs is more massive, the mass differences are small. While it would therefore be possible to observe these systems in transition given our simple model framework, is it likely? To investigate this question, we consider all pairs with mass differences of $\Delta M_* < 0.02M_\odot$. We assume that we cannot know a mass difference to better than this threshold due to the systematics described above, and hence the probability of observing any of these 18 roughly equal-mass pairs in transition is equally likely. We substitute $0.02M_\odot$ for ΔM_* into Equation 3, yielding 3.86% as a conservative estimate of the likelihood of each of these systems being observed in transition; note that this corresponds to a difference in spindown epoch of 0.31Gyr. Using binominal statistics, we find an 85% chance that we would have observed fewer transition pairs among the equal-mass binaries than the two that we did. While stellar mass is therefore the dominant effect in determining when a given star spins down (when metallicity and birth environment are controlled), our results hint that second-order effects may also be present; this could be explained by, for example, a 0.5Gyr dispersion in spindown epoch, which we found was plausibly consistent with our population-level results in the previous section. That said, there is still a 15% chance that the data are consistent with the simple model; however, this agreement requires the assumption that we cannot know a mass to better than $0.02M_\odot$, and a less conservative assumption would worsen the disagreement.

3.3. Commentary on the transition systems

The eight transition systems are exciting targets for future follow up work, representing pre- and post-spindown laboratories that are controlled for confounding variables such as differences in metallicity, birth environment, and age. Two of the systems are equal-mass binaries and hence even more exciting, as they are also controlled for stellar mass. In this section, we summarize the current state of knowledge on these systems; Figure 8 shows our TRES observations of H α .

3.3.1. 2MASS J11231269+8009027A and 2MASS J11231650+8009045B

2MA1123+80AB is an equal-mass pair with masses of $0.15M_\odot$, separated by $10''$ and located at 26pc, which yields a projected physical separation of 260au. We do not observe rotational broadening in our TRES spectra of either star, implying $v \sin i < 3.4 \text{ km s}^{-1}$. We observe H α emission of A in our FAST spectrum and two TRES spectra, taken in 2023 January, February, and April, respectively; it is therefore unlikely that we simply caught a quiescent star during a flare on three separate occasions. The pair appears at nearly identical magnitudes and colors in Figure 7, with the A component being marginally brighter and redder.

From our TRES observations, we measure radial velocities of $-17.0 \pm 0.5 \text{ km s}^{-1}$ for A and $-17.9 \pm 0.5 \text{ km s}^{-1}$ for B. The errors in these measurements are dominated by the uncertainty in absolute RV of a Barnard’s Star template that we use to calibrate our absolute RV scale; the differences between A and B are therefore statistically significant and likely reflect the mutual acceleration of the binary. We do not observe statistically significant

variation between our two observations of A that are separated by two months and have relative RV uncertainties of 60ms^{-1} .

While the pair has been observed in many TESS sectors, we are unable to identify one or more rotation periods from the blended light curve.

3.3.2. *2MASS J10204884-0633195A and 2MASS J10205111-0634400B*

2MA1020-06AB is a nearly equal-mass pair with masses of $0.26M_{\odot}$ and $0.24M_{\odot}$. The components are separated by $87''$ and located at 31pc, yielding a projected physical separation of 2700au. The system was previously identified as a cpm pair in [Boyd et al. \(2011\)](#), who refer to the pair as SCR J1020-0633A and SCR J1020-0634B.

Neither star shows rotational broadening in our TRES spectra, implying $v \sin i < 3.4\text{kms}^{-1}$. The stars are resolved separately by TESS; inspecting the TESS light curve of 2MA1020-06A, we find a rotation period of 3.8 days. We are unable to identify a period in the light curve of B. Our photometric and spectroscopic observations are consistent: using the [Boyajian et al. \(2012\)](#) mass–radius relation, we predict an equatorial velocity of 3.6kms^{-1} for A given a 3.8-day rotation period, which would result in undetectable rotational broadening for most values of $\sin i$. We measure a radial velocity of $16.4 \pm 0.5\text{kms}^{-1}$ for A and $16.3 \pm 0.5\text{kms}^{-1}$ for B.

Intriguingly, the BANYAN Σ tool ([Gagné et al. 2018](#)) finds that these stars’ galactic space motions are consistent with the Carina-Near Moving Group, with a membership probability of 99.7%. This result was previously reported in [Stahl et al. \(2022\)](#), who also measured $\text{H}\alpha$ equivalent widths for these stars and obtained measurements consistent with our findings. Carina-Near has an age of 200Myr ([Zuckerman et al. 2006](#)); such a young age for 2MA1020-06B would be incredibly surprising given its $\text{H}\alpha$ absorption. For this reason, [Stahl et al. \(2022\)](#) argue that this star is not a true member of Carina-Near despite its high membership probability. Instead, they suggest that its misclassification is the result of the kinematics of Carina-Near being poorly defined in BANYAN Σ , as only 13 members of this association were previously known. [Stahl et al. \(2022\)](#) do not acknowledge the binarity of 2MA1020-06AB and so they still consider 2MA1020-06A to be a Carina-Near member, as it does have $\text{H}\alpha$ emission, but the same misclassification argument would apply to both stars.

3.3.3. *2MASS J18524373+3659257A and 2MASS J18524397+3659176B*

2MA1852+36AB consists of stars with masses of $0.16M_{\odot}$ and $0.13M_{\odot}$, separated by $9''$ at a distance of

23pc. These values imply a physical projected separation of 210au. A is inactive in $\text{H}\alpha$ while the B component is active.

We observe a weak 1.7-day rotation period in the blended TESS light curve, presumably originating from the active B component. Neither star exhibits rotational broadening in our TRES spectra, but a non-detection could be consistent with a 1.7-day rotation period for B if $i < 40^{\circ}$. We measure a radial velocity of $-19.4 \pm 0.5\text{kms}^{-1}$ for A and $-19.8 \pm 0.5\text{kms}^{-1}$ for B.

3.3.4. *2MASS J01232866+6411443A and 2MASS J01233090+6411440B*

This system is a known cpm pair, referred to as UC 13 in the USNO CCD Astrographic Catalog (UCAC; [Caballero 2010](#); [Hartkopf et al. 2013](#)). It comprises $0.31M_{\odot}$ and $0.27M_{\odot}$ stars separated by $15''$. At a distance of 32pc, this corresponds to a physical projected separation of 480au. A is inactive in $\text{H}\alpha$ while the B component is active.

Neither star shows rotational broadening in our TRES spectra, nor do we observe a rotation period in the blended TESS light curve. We measure radial velocities of $-7.3 \pm 0.5\text{kms}^{-1}$ for A and $-7.7 \pm 0.5\text{kms}^{-1}$ for B.

3.3.5. *2MASS J14593063+2833387A and 2MASS J14593085+2833463B*

This pair appears in the Luyten Double Star catalog as LDS 6302AB ([Luyten 1995](#)). It consists of $0.21M_{\odot}$ and $0.16M_{\odot}$ stars, separated by $8''$ and at a distance of 33pc, yielding a projected physical separation of 260au. A is inactive in $\text{H}\alpha$ while the B component is active.

Like the previous system, neither star shows rotational broadening nor do we observe a rotation period in the blended TESS light curve. We measure radial velocities of $11.8 \pm 0.5\text{kms}^{-1}$ for A and $11.6 \pm 0.5\text{kms}^{-1}$ for B.

3.3.6. *2MASS J20350677+0218289A and 2MASS J20350608+0218166B*

This pair appears as a cpm pair in the UCAC with designation UC 4224AB ([Hartkopf et al. 2013](#)). The components have masses of $0.29M_{\odot}$ and $0.19M_{\odot}$. They are separated by $16''$ and located at 20pc, yielding a projected physical separation of 320au. A is inactive in $\text{H}\alpha$ while the B component is active.

We again do not observe any rotational broadening in our TRES spectra nor a rotation period in the blended TESS light curve. We measure radial velocities of $7.0 \pm 0.5\text{kms}^{-1}$ for A and $7.4 \pm 0.5\text{kms}^{-1}$ for B.

3.3.7. *2MASS J16552527-0819207A and 2MASS J16553529-0823401B*

Our penultimate transition pair is known by many names, including Gl 643 and Gl 644C. This pair is part

of a quintuple star system, with both components widely separated from each other and from the close triple, Gl 644, which is itself composed of three M dwarfs (Mazeh et al. 2001). We did not observe the triple in this study.

The two stars we did observe have masses of $0.21M_{\odot}$ and $0.09M_{\odot}$ and are separated by $299''$. As they are located at only 6pc, this corresponds to a projected physical separation of 1800au. Gl 643 is inactive in H α while Gl 644C is active.

The pair has not been observed by TESS, but Díez Alonso et al. (2019) report a rotation period of 6.5 days for the more massive component based on ASAS photometry (Pojmanski 1997). Such a short rotation period would be highly unusual for a fully convective M dwarf with H α in absorption, with rotation periods of 95 ± 22 days being typical for inactive M dwarfs at this mass (Newton et al. 2017), but perhaps could reflect the special phase of the star’s life in which we are observing these transition systems. We do not observe a signal with this rotation period in 4559 observations from the MEarth Project (Nutzman & Charbonneau 2008; Irwin et al. 2015) taken between 2021 February–July, although we are also unable to identify a different period. Further observation of this target would be beneficial to establish whether it is truly a rapid rotator.

While Gl 643 does not exhibit rotational broadening in our TRES spectra, we measure $v \sin i$ of 6.1 km s^{-1} for Gl 644C. This broadening implies that the rotation period of this star is shorter than 1.2 days. A comparable value of $v \sin i = 5.4 \pm 1.5 \text{ km s}^{-1}$ was previously measured for this star with the higher-resolution ($R = 94600$) CARMENES-VIS spectrograph in Reiners et al. (2018). We observe a tentative 1.095-day rotation period in 3754 MEarth observations taken between 2014–2018, consistent with the observed rotational broadening, although this signal did not pass the significance threshold to be considered a robust detection in Newton et al. (2018).

We measure a radial velocity of $16.0 \pm 0.5 \text{ km s}^{-1}$ for Gl 643 and $14.5 \pm 0.5 \text{ km s}^{-1}$ for Gl 644C.

3.3.8. *2MASS J22261576+0300182A and 2MASS J22261549+0300075B*

The transition pair with the largest mass difference between components is 2MA2226+03AB, better known as LHS 3808 and LHS 3809, and designated as LDS 4967AB in the Luyten Double Star catalog (Luyten 1995). The primary has a mass of $0.33M_{\odot}$ and the secondary has a mass of $0.14M_{\odot}$. The components are separated by $12''$, which at a distance of 23pc corresponds to a projected physical separation of 280au.

We discussed this pair in a previous investigation, Pass et al. (2022), as both components have rotation periods measured from MEarth photometry (Newton et al.

2016): 94 days for the inactive LHS 3808 and 1.6 days for the active LHS 3809. With our new TRES spectra, we measure rotational broadening of $v \sin i = 5.0 \text{ km s}^{-1}$ for LHS 3809 and no measurable broadening for LHS 3808 at the resolution of the spectrograph. A 1.6-day rotation period for LHS 3809 yields an equatorial velocity of 5.8 km s^{-1} , consistent with our $v \sin i$ measurement for a modest inclination. We measure RVs of $-1.3 \pm 0.5 \text{ km s}^{-1}$ for LHS 3808 and $-1.7 \pm 0.5 \text{ km s}^{-1}$ for LHS 3809.

4. SUMMARY AND CONCLUSIONS

We constructed a sample of 67 wide, fully convective M-dwarf binaries using Gaia kinematics and measured H α equivalent widths for each component with FAST, a mid-resolution optical spectrograph. We classified pairs as active, inactive, or transition based on the equivalent widths of their H α features. We then followed up candidate transition systems using higher-resolution spectroscopy to vet them for unresolved binaries. Ultimately, we found 22 systems in which both components are active, 36 systems in which both are inactive, 8 transition systems with one active and one inactive component, and 1 newly discovered triple, LDS 942AC-B.

We gathered ten epochs of spectra for LDS 942AC with the $R = 44000$ TRES spectrograph in order to fit the orbit of this new double-lined spectroscopic binary. We found that the pair orbits with a period of 25 days and is substantially eccentric. Intriguingly, the most massive star in the LDS 942 system is the widely separated B component, which is also highly H α active. The A component is less massive with modest H α emission, and the C component is least massive with no measurable H α emission. Many examples are known in which an M dwarf in a close binary has its H α emission and rapid rotation persist to advanced ages due to interactions between the binary components. This system suggests that an opposite effect may also be possible: while we typically expect the more massive component to spin down first, interactions between the A and C component may have caused them to spin down at a younger age.

Next, we presented an empirical relationship to estimate the average epoch of spindown for fully convective M dwarfs (Equation 2), which is the mass-dependent age of transition between the active/rapidly rotating mode and the inactive/quiescent one. This equation is based on a volume-complete sample of 323 single, 0.1 – $0.3M_{\odot}$ M dwarfs that we studied in Pass et al. (2023a,b) and hence should only be applied to fully convective M dwarfs. Using this relationship, we analyzed our wide binary sample to determine if our observations were consistent with the epoch of spindown being dependent on stellar mass alone, specifically for these systems in which

metallicity and birth environment are presumably the same for both components.

We observed more active pairs and fewer inactive pairs than we naively expected, and determined that biases due to youth or unresolved binarity were unlikely to explain the discrepancy. However, the observed distribution of systems was consistent with dynamical processing, with the population of wide binaries dwindling with age due to gravitational perturbations by passing stars causing some binaries to be disrupted. Accounting for this effect, we found that the fraction of transition pairs was consistent with the spindown epoch depending on stellar mass alone; however, the number of equal-mass binaries that were transition systems was marginally higher than expected, suggesting that some second-order effects may also be present. A stochastic component with a dispersion of $\leq 0.5\text{Gyr}$ (or $\leq 25\%$) would be consistent with our population-level observations. While we refer to this component as stochastic, it is not necessarily random; rather, such a dispersion could result from deterministic but unknown differences in the early evolution of the stars, such as the influence of planet formation.

When controlling for metallicity and birth environment, the epoch of spindown for fully convective M dwarfs is therefore predominately determined by stellar mass. However, we know that for a given stellar mass, there is significant dispersion in the spindown epochs of field stars: in [Pass et al. \(2022\)](#), we identified a sample of $0.3M_{\odot}$ stars that had spun down by 600Myr, while Equation 2 yields a typical spindown epoch of 1.3Gyr for this mass. Further work to quantify the dispersion in the field sample is necessary to determine whether the field’s star-to-star variation exceeds the stochastic component allowed by our observations of M-M binary pairs. If the field sample has a larger dispersion, it would imply that the dominant source of variation is not stochastic, but rather based on factors that are shared between members of our wide binary pairs. For example, the high-energy birth environment may determine the circumstellar disk lifetime, and hence, the length of the disk-locking phase and the initial rotation of the star following disk dissipation ([Roquette et al. 2021](#)). Such a result could follow from magnetic-morphology-driven spindown ([Garraffo et al. 2018](#); [Monsch et al. 2023](#)), in which the epoch of spindown is determined entirely by initial rotation rate and stellar mass, or the [Matt et al. \(2015\)](#) torque law, which similarly depends on these pa-

rameters. A significant environmental influence would also be consistent with observations of cluster-to-cluster variance in the distribution of stellar rotation rates (e.g., [Coker et al. 2016](#)). Given such cluster observations, it is likely reasonable to assume that initial rotation rate has both an environmental and individual component, with the high-energy birth environment shared between the two stars in our binaries playing a role, as well as differences in the early evolution of each star.

We reported the properties of our stars in Tables A1, A2, and A3. Our eight transition systems are exciting targets for further study, representing pre- and post-spindown laboratories that are controlled for confounding variables such as differences in metallicity, birth environment, and age—and in the case of the two equal-mass binaries, also mass. To facilitate future work on these systems, we concluded by summarizing previous observations of these stars from the literature, as well as new inferences from TESS photometry and our TRES spectroscopy.

ACKNOWLEDGEMENTS

We thank Allyson Bieryla, Warren Brown, Lars Buchhave, Pascal Fortin, Jonathan Irwin, Sean Moran, Samuel Quinn, Andrew Szentgyorgyi, and Jennifer Winters for their contributions to FAST/TRES operations and/or code development.

This paper uses data products produced by the OIR Telescope Data Center, supported by the Smithsonian Astrophysical Observatory; the Two Micron All Sky Survey, which is a joint project of the University of Massachusetts and the Infrared Processing and Analysis Center/California Institute of Technology funded by the National Aeronautics and Space Administration and the National Science Foundation; the TESS mission, with funding provided by NASA’s Science Mission Directorate and public data processed at the TESS Science Office and the TESS Science Processing Operations Center; and the European Space Agency (ESA) mission Gaia, processed by the Gaia Data Processing and Analysis Consortium (DPAC). Funding for the DPAC has been provided by national institutions, in particular the institutions participating in the Gaia Multilateral Agreement. EP is supported in part by a Natural Sciences and Engineering Research Council of Canada (NSERC) Postgraduate Scholarship.

Facilities: FLWO:1.5m (FAST/TRES), Gaia

REFERENCES

- Benedict, G. F., Henry, T. J., Franz, O. G., et al. 2016, [AJ](#), 152, 141
- Boyajian, T. S., von Braun, K., van Belle, G., et al. 2012, [ApJ](#), 757, 112

- Boyd, M. R., Winters, J. G., Henry, T. J., et al. 2011, *AJ*, **142**, 10
- Brandt, T. D. & Huang, C. X. 2015, *ApJ*, **807**, 24
- Caballero, R. 2010, *JDSO*, **6**, 97
- Coker, C. T., Pinsonneault, M., & Terndrup, D. M. 2016, *ApJ*, **833**, 122
- Covey, K. R., Agüeros, M. A., Law, N. M., et al. 2016, *ApJ*, **822**, 81
- Cutri, R. M., Skrutskie, M. F., van Dyk, S., et al. 2003, *VizieR Online Data Catalog*, **II/246**
- Desidera, S., Gratton, R. G., Lucatello, S., & Claudi, R. U. 2006, *A&A*, **454**, 581
- Desidera, S., Gratton, R. G., Scuderi, S., et al. 2004, *A&A*, **420**, 683
- Díez Alonso, E., Caballero, J. A., Montes, D., et al. 2019, *A&A*, **621**, A126
- Fabricant, D., Cheimets, P., Caldwell, N., & Geary, J. 1998, *PASP*, **110**, 79
- Fantin, N. J., Côté, P., McConnachie, A. W., et al. 2019, *ApJ*, **887**, 148
- Felce, C. & Fuller, J. 2023, *MNRAS*, **526**, 6168
- Foreman-Mackey, D., Luger, R., Agol, E., et al. 2021, *JOSS*, **6**, 3285
- France, K., Arulanantham, N., Fossati, L., et al. 2018, *ApJS*, **239**, 16
- Gagné, J., Mamajek, E. E., Malo, L., et al. 2018, *ApJ*, **856**, 23
- Gaia Collaboration, Brown, A. G. A., Vallenari, A., et al. 2021, *A&A*, **649**, A1
- Gaia Collaboration, Prusti, T., de Bruijne, J. H. J., et al. 2016, *A&A*, **595**, A1
- Garraffo, C., Drake, J. J., Dotter, A., et al. 2018, *ApJ*, **862**, 90
- Hartkopf, W. I., Mason, B. D., Finch, C. T., et al. 2013, *AJ*, **146**, 76
- Heggie, D. C. 1975, *MNRAS*, **173**, 729
- Irwin, J. M., Berta-Thompson, Z. K., Charbonneau, D., et al. 2015, in 18th Cambridge Workshop on Cool Stars, Stellar Systems, and the Sun, Cambridge Workshop on Cool Stars, Stellar Systems, and the Sun, **767–772**
- Irwin, J. M., Quinn, S. N., Berta, Z. K., et al. 2011, *ApJ*, **742**, 123
- Jackson, R. J. & Jeffries, R. D. 2013, *MNRAS*, **431**, 1883
- Jiang, Y.-F. & Tremaine, S. 2010, *MNRAS*, **401**, 977
- Kiraga, M. & Stepien, K. 2007, *AcA*, **57**, 149
- Lammer, H., Lichtenegger, H. I. M., Kulikov, Y. N., et al. 2007, *Astrobiology*, **7**, 185
- Lindgren, L., Klioner, S. A., Hernández, J., et al. 2021, *A&A*, **649**, A2
- Longmore, S. N., Kruijssen, J. M. D., Bastian, N., et al. 2014, in Protostars and Planets VI, ed. H. Beuther, R. S. Klessen, C. P. Dullemond, & T. Henning, **291–314**
- Lovis, C., Snellen, I., Mouillet, D., et al. 2017, *A&A*, **599**, A16
- Luyten, W. J. 1969, Proper Motion Survey, University of Minnesota, **21**, 1
- Luyten, W. J. 1995, *VizieR Online Data Catalog*, **I/98A**
- Marrese, P. M., Marinoni, S., Fabrizio, M., & Altavilla, G. 2019, *A&A*, **621**, A144
- Matt, S. P., Brun, A. S., Baraffe, I., Bouvier, J., & Chabrier, G. 2015, *ApJL*, **799**, L23
- Mazeh, T., Latham, D. W., Goldberg, E., et al. 2001, *MNRAS*, **325**, 343
- Medina, A. A., Charbonneau, D., Winters, J. G., Irwin, J., & Mink, J. 2022a, *ApJ*, **928**, 185
- Medina, A. A., Winters, J. G., Irwin, J. M., & Charbonneau, D. 2020, *ApJ*, **905**, 107
- Medina, A. A., Winters, J. G., Irwin, J. M., & Charbonneau, D. 2022b, *ApJ*, **935**, 104
- Miyakawa, K., Hirano, T., Fukui, A., et al. 2021, *AJ*, **162**, 104
- Moeckel, N. & Clarke, C. J. 2011, *MNRAS*, **415**, 1179
- Monsch, K., Drake, J. J., Garraffo, C., Picogna, G., & Ercolano, B. 2023, *ApJ*, **959**, 140
- Montes, D., González-Peinado, R., Tabernero, H. M., et al. 2018, *MNRAS*, **479**, 1332
- Morley, C. V., Kreidberg, L., Rustamkulov, Z., Robinson, T., & Fortney, J. J. 2017, *ApJ*, **850**, 121
- Morrell, S. & Naylor, T. 2019, *MNRAS*, **489**, 2615
- Newton, E. R., Irwin, J., Charbonneau, D., et al. 2017, *ApJ*, **834**, 85
- Newton, E. R., Irwin, J., Charbonneau, D., et al. 2016, *ApJ*, **821**, 93
- Newton, E. R., Mondrik, N., Irwin, J., Winters, J. G., & Charbonneau, D. 2018, *AJ*, **156**, 217
- Nutzman, P. & Charbonneau, D. 2008, *PASP*, **120**, 317
- Parker, R. J. & Meyer, M. R. 2014, *MNRAS*, **442**, 3722
- Pass, E. K. & Charbonneau, D. 2023, *ApJ*, **949**, 37
- Pass, E. K., Charbonneau, D., Irwin, J. M., & Winters, J. G. 2022, *ApJ*, **936**, 109
- Pass, E. K., Winters, J. G., Charbonneau, D., et al. 2023a, *AJ*, **166**, 11
- Pass, E. K., Winters, J. G., Charbonneau, D., Irwin, J. M., & Medina, A. A. 2023b, *AJ*, **166**, 16
- Pojmanski, G. 1997, *AcA*, **47**, 467
- Rebull, L. M., Stauffer, J. R., Cody, A. M., et al. 2018, *AJ*, **155**, 196
- Reiners, A., Zechmeister, M., Caballero, J. A., et al. 2018, *A&A*, **612**, A49

- Ricker, G. R., Winn, J. N., Vanderspek, R., et al. 2015, [JATIS](#), **1**, 014003
- Riedel, A. R., Finch, C. T., Henry, T. J., et al. 2014, [AJ](#), **147**, 85
- Roquette, J., Matt, S. P., Winter, A. J., Amard, L., & Stasevic, S. 2021, [MNRAS](#), **508**, 3710
- Salvatier, J., Wiecki, T. V., & Fonnesbeck, C. 2016, *PeerJ Computer Science*, **2**, 2
- Skumanich, A. 1972, [ApJ](#), **171**, 565
- Snellen, I. A. G., de Kok, R. J., le Poole, R., Brogi, M., & Birkby, J. 2013, [ApJ](#), **764**, 182
- Somers, G., Cao, L., & Pinsonneault, M. H. 2020, [ApJ](#), **891**, 29
- Stahl, A. G., Johns-Krull, C. M., & Flagg, L. 2022, [ApJ](#), **941**, 101
- Tilley, M. A., Segura, A., Meadows, V., Hawley, S., & Davenport, J. 2019, [Astrobiology](#), **19**, 64
- Tokarz, S. P. & Roll, J. 1997, in *Astronomical Society of the Pacific Conference Series*, Vol. 125, *Astronomical Data Analysis Software and Systems VI*, ed. G. Hunt & H. Payne, 140
- West, A. A., Weisenburger, K. L., Irwin, J., et al. 2015, [ApJ](#), **812**, 3
- Winters, J. G., Charbonneau, D., Henry, T. J., et al. 2021, [AJ](#), **161**, 63
- Winters, J. G., Henry, T. J., Jao, W.-C., et al. 2019, [AJ](#), **157**, 216
- Winters, J. G., Irwin, J. M., Charbonneau, D., et al. 2020, [AJ](#), **159**, 290
- Wright, N. J., Drake, J. J., Mamajek, E. E., & Henry, G. W. 2011, [ApJ](#), **743**, 48
- Wright, N. J., Newton, E. R., Williams, P. K. G., Drake, J. J., & Yadav, R. K. 2018, [MNRAS](#), **479**, 2351
- Zucker, S. & Mazeh, T. 1994, [ApJ](#), **420**, 806
- Zuckerman, B., Bessell, M. S., Song, I., & Kim, S. 2006, [ApJL](#), **649**, L115

APPENDIX

A. LONG TABLES

Table A1. Transition systems

2MASS A	2MASS B	d [pc]	ρ ["]	M_A [M_\odot]	M_B [M_\odot]	ΔM [M_\odot]	FAST-H α_A [\AA]	FAST-H α_B [\AA]	TRES-H α_A [\AA]	TRES-H α_B [\AA]
11231269+8009027	11231650+8009045	26	10	0.151	0.150	0.002	-0.695 \pm 0.058	-0.151 \pm 0.060	-1.691	-0.192
10204884-0633195	10205111-0634400	31	87	0.256	0.240	0.016	-3.571 \pm 0.044	0.020 \pm 0.026	-3.746	0.064
18524373+3659257	18524397+3659176	23	9	0.161	0.130	0.031	-0.041 \pm 0.034	-1.598 \pm 0.057	-0.196	-1.765
01232866+6411443	01233090+6411440	32	15	0.312	0.270	0.042	0.106 \pm 0.028	-1.279 \pm 0.025	0.074	-1.687
14593063+2833387	14593085+2833463	33	8	0.209	0.157	0.052	0.018 \pm 0.032	-2.712 \pm 0.054	0.049	-2.207
20350677+0218289	20350608+0218166	20	16	0.295	0.188	0.107	0.074 \pm 0.041	-3.982 \pm 0.042	-0.014	-4.049
16552527-0819207	16553529-0823401	6	299	0.211	0.091	0.120	0.173 \pm 0.017	-4.863 \pm 0.075	0.071	-6.605
22261576+0300182	22261549+0300075	23	12	0.332	0.135	0.196	0.017 \pm 0.024	-4.669 \pm 0.123	0.084	-6.035

Table A2. Active systems

2MASS A	2MASS B	d [pc]	ρ ["]	M_A [M_\odot]	M_B [M_\odot]	ΔM [M_\odot]	FAST-H α_A [\AA]	FAST-H α_B [\AA]	TRES-H α_A [\AA]	TRES-H α_B [\AA]
22353648+0032374	22353647+0032332	41	4	0.286	0.285	0.001	-4.925 \pm 0.061	-3.539 \pm 0.063		
12212705+3038357	12212673+3038376	12	4	0.125	0.123	0.002	-5.109 \pm 0.040	-4.704 \pm 0.044		
04331742+6846543	04331837+6846573	19	6	0.131	0.127	0.004	-3.656 \pm 0.060	-2.088 \pm 0.061		
06141246-1436023	06141237-1436085	26	6	0.212	0.207	0.005	-2.889 \pm 0.058	-2.007 \pm 0.058		
19522690+3155187	19522688+3158119	33	173	0.309	0.304	0.005	-3.811 \pm 0.052	-5.585 \pm 0.058		
14022709+1520339	14022674+1520384	35	7	0.283	0.277	0.006	-4.808 \pm 0.062	-6.072 \pm 0.074		
14275607-0022310	14275640-0022191	18	13	0.278	0.269	0.009	-9.067 \pm 0.057	-9.289 \pm 0.057		
09191895+3831159	09191904+3831233	19	7	0.214	0.203	0.011	-5.407 \pm 0.032	-4.722 \pm 0.032		
04283289+4157240	04283205+4157239	47	9	0.273	0.261	0.012	-14.713 \pm 0.071	-4.372 \pm 0.059		
03595303+1325443	03595281+1325415	34	4	0.287	0.270	0.018	-3.924 \pm 0.053	-5.768 \pm 0.048		
21523313+1147445	21523345+1147460	50	5	0.316	0.289	0.027	-5.913 \pm 0.065	-16.596 \pm 0.103		
17274706+5200018	17274680+5200079	29	6	0.232	0.203	0.029	-6.827 \pm 0.049	-8.524 \pm 0.060		
10241364+3902333	10241320+3902304	18	6	0.258	0.224	0.034	-2.958 \pm 0.029	-3.577 \pm 0.034		
13360002+4024118	13355969+4021459	24	5	0.178	0.141	0.037	-4.924 \pm 0.033	-7.021 \pm 0.061		
00095737-0636149	00095982-0632010	35	256	0.269	0.227	0.042	-4.582 \pm 0.051	-4.939 \pm 0.066		
02090447+4341267	02090486+4341250	37	5	0.327	0.284	0.043	-5.703 \pm 0.061	-2.820 \pm 0.063		
02230174+6600452	02230030+6600446	42	9	0.215	0.168	0.046	-6.089 \pm 0.079	-4.976 \pm 0.130		
02032589+0648008	02033222+0648588	24	111	0.271	0.211	0.060	-0.785 \pm 0.025	-2.714 \pm 0.036	-1.465	-2.423
12332604+5226589	12332593+5227167	46	18	0.308	0.239	0.069	-5.979 \pm 0.042	-5.644 \pm 0.073		
23204335+8329513	23204037+8329463	46	7	0.289	0.220	0.069	-3.635 \pm 0.090	-5.139 \pm 0.094		
09234719+6357447	09234740+6357387	32	6	0.278	0.164	0.115	-4.917 \pm 0.038	-3.977 \pm 0.045		
03513447+0722250	03513420+0722229	36	5	0.298	0.169	0.129	-4.018 \pm 0.075	-6.169 \pm 0.142		

Table A3. Inactive systems

2MASS A	2MASS B	d [pc]	ρ ["]	M_A [M_\odot]	M_B [M_\odot]	ΔM [M_\odot]	FAST-H α_A [Å]	FAST-H α_B [Å]	TRES-H α_A [Å]	TRES-H α_B [Å]
06492207+3209599	06492214+3209551	31	5	0.236	0.235	0.001	-0.008±0.038	0.050±0.041		
19071320+2052372	19070556+2053168	9	114	0.346	0.345	0.001	0.037±0.010	0.045±0.010		
20252724+5433327	20252445+5433458	32	28	0.316	0.312	0.005	0.077±0.038	0.114±0.038		
22113258+0058490	22113228+0058514	34	5	0.265	0.258	0.007	0.189±0.029	0.127±0.030		
01431772-0151223	01431760-0151265	47	5	0.227	0.214	0.013	-0.080±0.053	-0.894±0.061	-0.388	-0.390
14452674-1311353	14452576-1311495	33	20	0.308	0.292	0.015	-0.003±0.033	0.128±0.035		
10260265+5027090	10260331+5027220	19	14	0.301	0.277	0.023	0.026±0.042	0.010±0.046		
12204478-0451408	12204459-0451456	34	6	0.238	0.213	0.024	0.060±0.036	0.036±0.043		
19384867+3512361	19384898+3512370	34	4	0.168	0.144	0.024	0.752±0.044	0.507±0.091		
14364366-0830245	14364401-0830305	44	8	0.330	0.305	0.025	0.032±0.052	0.113±0.059		
02513445+5922325	02513375+5922349	36	6	0.263	0.236	0.026	-0.153±0.042	-0.205±0.053		
13102287+3155167	13102342+3155159	50	7	0.322	0.292	0.030	-0.112±0.030	0.118±0.044		
03263459+3929072	03263418+3929029	19	7	0.242	0.210	0.032	0.362±0.025	0.252±0.030		
02541919+6427401	02542325+6425552	43	108	0.312	0.277	0.035	0.023±0.047	-0.173±0.100		
18251482+0721284	18250818+0721482	37	101	0.341	0.306	0.036	0.201±0.031	0.335±0.035		
14022402-0312001	14022282-0312217	32	28	0.198	0.159	0.039	0.038±0.050	0.141±0.057		
21334913+0146561	21334914+0147012	17	5	0.213	0.173	0.040	0.082±0.027	0.083±0.029		
23580162+7836301	23575233+7836458	26	32	0.307	0.266	0.041	0.070±0.031	0.199±0.038		
02330114+0105389	02330063+0106070	45	29	0.257	0.211	0.046	0.039±0.057	-0.170±0.078		
18115228+3225199	18115554+3225466	28	49	0.194	0.145	0.049	0.063±0.058	-0.012±0.054		
20563492+3047518	20563466+3047425	33	10	0.293	0.241	0.052	0.073±0.028	0.074±0.033		
10230158-0735092	10230164-0735248	37	16	0.235	0.183	0.053	-0.075±0.044	-0.081±0.053		
00515271+3750216	00515693+3751159	38	74	0.279	0.225	0.054	0.056±0.052	-0.137±0.068		
22585768+6430048	22573941+6418533	48	841	0.332	0.255	0.078	0.083±0.039	0.257±0.052		
22282013+0303534	22281858+0303424	49	26	0.305	0.224	0.081	0.196±0.043	0.432±0.063		
10191279-0305520	10191244-0305519	46	5	0.252	0.165	0.087	0.139±0.048	-0.017±0.040		
15400352+4329396	15400374+4329355	13	4	0.295	0.204	0.091	0.334±0.012	0.134±0.032		
21440900+1703348	21440795+1704372	17	64	0.264	0.171	0.093	0.154±0.037	-0.079±0.059		
12114753+2400064	12114707+2400054	40	7	0.253	0.158	0.096	0.296±0.034	0.238±0.080		
11485296+1800581	11485323+1800564	42	4	0.347	0.249	0.098	0.143±0.052	-0.078±0.047		
04281667+0600130	04281665+0600176	24	5	0.260	0.130	0.130	0.071±0.040	-0.198±0.084		
02274112+0613539	02274066+0613550	40	7	0.330	0.189	0.141	0.047±0.061	-0.146±0.095		
14515365+5147107	14515297+5147134	33	7	0.284	0.136	0.148	0.313±0.031	0.370±0.050		
18180427+3846342	18180345+3846359	11	10	0.318	0.165	0.152	0.165±0.019	0.093±0.022		
15352059+1742470	15352039+1743045	15	18	0.297	0.129	0.168	0.117±0.016	0.036±0.038		
19445022-0203562	19444998-0203534	37	5	0.345	0.161	0.184	0.315±0.044	0.133±0.059		